
LESS IS MORE: THE INFLUENCE OF PRUNING ON THE EXPLAINABILITY OF CNNs

A PREPRINT

 **Florian Merkle**
 Innsbruck University
 Department of Information Systems, Production
 and Logistics Management
 Austria
 florian.merkle@student.uibk.ac.at

 **David Weber**
 MCI – The Entrepreneurial School
 Innsbruck
 Austria
 weber_david@outlook.com

 **Pascal Schöttle**
 Josef Ressel Centre for Security Analysis of IoT Devices
 Innsbruck
 Austria
 pascal.schoettle@mci.edu

 **Stephan Schlögl**
 MCI – The Entrepreneurial School
 Innsbruck
 Austria
 stephan.schloegl@mci.edu

 **Martin Nocker**
 Josef Ressel Centre for Security Analysis of IoT Devices
 Innsbruck
 Austria
 martin.nocker@mci.edu

January 10, 2025

ABSTRACT

Over the last century, deep learning models have become the state-of-the-art for solving complex computer vision problems. These modern computer vision models have millions of parameters, which presents two major challenges: (1) the increased computational requirements hamper the deployment in resource-constrained environments, such as mobile or IoT devices, and (2) explaining the complex decisions of such networks to humans is challenging. Network pruning is a technical approach to reduce the complexity of models, where less important parameters are removed. The work presented in this paper investigates whether this reduction in technical complexity also helps with perceived explainability. To do so, we conducted a pre-study and two human-grounded experiments, assessing the effects of different pruning ratios on explainability. Overall, we evaluate four different compression rates (i.e., 2, 4, 8, and 32) with 37 500 tasks on Mechanical Turk. Results indicate that lower compression rates have a positive influence on explainability, while higher compression rates show negative effects. Furthermore, we were able to identify sweet spots that increase both the perceived explainability and the model's performance.

Keywords machine learning · deep learning · explainable artificial intelligence · neural network pruning · internet of things

1 Introduction

Today's products and services increasingly benefit from integrating ever more powerful machine learning (ML) features. In particular, the use of deep learning and respective deep neural networks (DNN) has significantly expanded upon the capabilities of intelligent systems and consequently improved the performance of autonomous vehicles, virtual assistants,

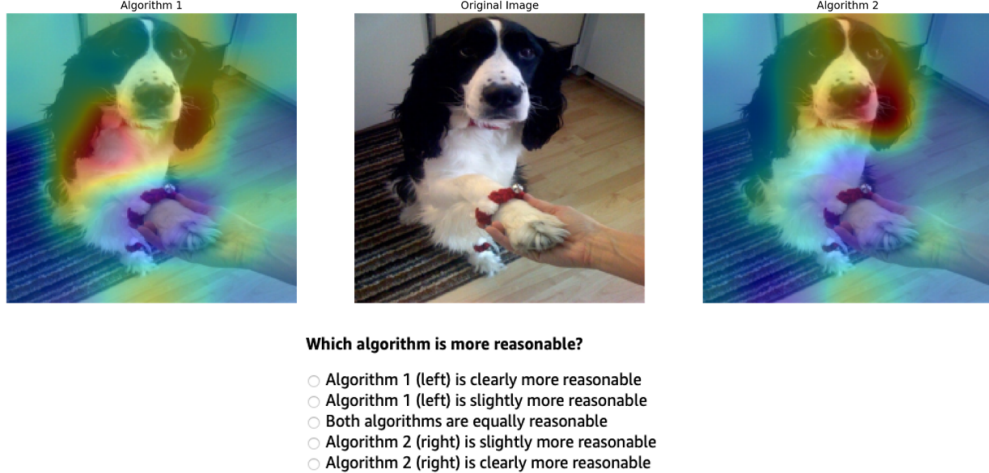


Figure 1: Which algorithm is more reasonable? In the middle, we show the original picture; on the left, the explainability heat map of compression rate 1; and on the right, the explainability heat map for compression rate 8. Red colors indicate more important regions, while blue colors indicate less important regions.

fraud detection software, and tools that make heavy use of image recognition technology. Concrete application domains for these DNNs are found, e.g., in medicine [1], production [2], cyber security [3] and finance [4]. To this end, convolutional neural networks (CNN) – a particular type of DNN – have demonstrated great performance in computer vision tasks. This includes image classification of chest x-rays to treat COVID-19 patients [5], image segmentation of MRI scans to analyze different regions of the brain [6], or object detection to support autonomous driving [7].

These recent advancements in computer vision can be largely attributed to the increased availability of data and significant improvements in computational power, enabling the development of larger and more complex models [8]. This remains less problematic when energy and computational resources are readily available, i.e., the computation is performed on a workstation or in the cloud. However, computer vision systems are also deployed in resource-constrained settings such as mobile and smart devices or Internet of Things (IoT) applications. Moreover, many of these applications, such as smart doorbells and cameras [9], are privacy- or security-sensitive and rely on a certain level of trust from the users. Prior research indicates that explainable decisions increase users' trust towards deep learning model [10].

Therefore, this study aims to tackle the following limitations that today's DNNs (and consequently CNNs) face:

1. Complexity: State-of-the-art DNNs have to deal with millions of parameters and thus require large amounts of computing power and memory. This is especially important for applications in resource-constrained environments, such as smartphones and IoT devices. Furthermore, more parameters negatively influence the inference time, which is critical for real-time applications such as autonomous cars or face detection. One technical approach to retrospectively reduce DNN parameters is so-called neural network (NN) pruning, where less important parameters are deleted.
2. Explainability: DNNs experience a lack of explainability that leaves little understanding of why a particular decision was made [11]. Especially the structure of CNNs, consisting of complex internal relations, can be challenging to explain [12]. Understanding the reasoning of these systems is crucial, especially for high-stake decision-making and highly regulated domains. A DNN's decisions may determine the difference between life and death, as in healthcare, medicine, or autonomous driving. More explainable, reasonable, and transparent DNNs would increase trust, acceptance, and awareness in society.

Intuitively, more parameters, i.e., more complexity, lead to a lower explainability, as not every connection can be interpreted with human reasonability. This is clearly shown with DNNs, as their high number of parameters and complex internal sequences appear opaque to humans [13] and certain explainability methods are prone to produce noisy and indistinct explanations [14]. At the same time, this striving for complexity helped state-of-the-art NNs reach their current performance. In this paper, we start from the hypothesis that retrospectively reducing the number of parameters with the help of NN pruning can increase the explainability to humans.

We apply several network pruning compression rates (CR), i.e., CR 2, 4, 8, and 32, to a VGG-16 [15] network. VGG-16 is a common CNN architecture with a simple and homogeneous structure. Its size of 138 million parameters provides ideal preconditions for pruning and opaque behavior. Grad-CAM [16] is our explainability method of choice, as it

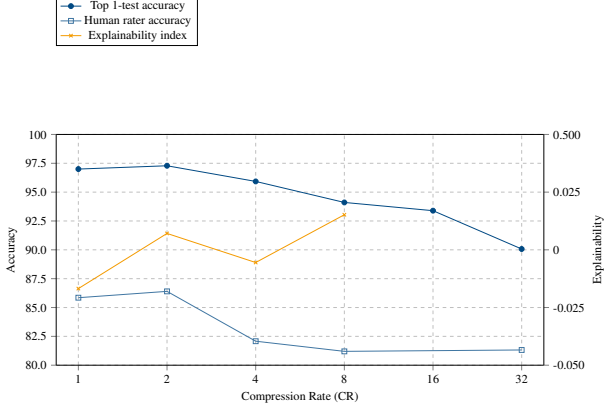


Figure 2: Top-1 test-set accuracies (dark blue, left y-axis), human rater accuracies (light blue, left y-axis), and our explainability measure (orange, right y-axis) for different compression rates.

allows for a visual explanation for the internal reasoning of black-box CNNs, passes several sanity checks by Adebayo et al. [17], and applies to any CNN architecture. We conduct three human-grounded experiments with 37 500 tasks on Amazon’s Mechanical Turk¹ platform. We analyze the data gathered from these experiments with evaluation metrics from both objective and subjective experiments, i.e., one where ground truth is given and one where ground truth is not given. Figure 1 shows the experimental setup of one of our experiments. Our results indicate a sweet spot of mild pruning, with a CR of 2, i.e., a CNN with half the parameters. As visible in Figure 2, not only does the top 1 test accuracy of the CNN improve, but also the evaluation metrics from both subjective (explainability index) and objective experiments (human-rater-accuracy). The remainder of this paper reports the details of this investigation.

We discuss the relevant theoretical background in Section 2. Next, we describe our methodological approach in Section 3. Section 4 then reports on respective results, Section 5 reflects on the limitations of our approach, and Section 6 highlights directions for future work. Finally, Section 7 summarizes and concludes the paper.

2 Theoretical Background

ML methods, particularly DNN approaches, are powerful tools for creating predictions based on data. Yet, they are often called black-box models, as their inner workings lack transparency. Even so, these non-transparent systems are increasingly used for high-stake decision-making in healthcare, precision medicine, criminal justice, autonomous driving, and other highly regulated domains impacting human lives [18, 19, 20]. Not being able to explain the system’s decisions thus poses evident dangers [21]. This implies that it is not enough to receive a prediction (i.e., the *what*) but also the explanation of how this prediction was made (i.e., the *why*). Or, as Doshi-Velez and Kim [22] emphasize, “*Explainability completes the problem formulation*”.

2.1 Explainability in Machine Learning

Unfortunately, ML literature lacks a clear definition of *explainability* and *interpretability*. Consequently, terms are regularly ill-defined, misused or referred to in different ways [23]. Also, it may happen that *explainability* and *interpretability* are used synonymously [24, 25], although Gilpin et al. [26] clearly state that *interpretability* (i.e., human-understandability) and *fidelity* (i.e., the accurate description of a system’s internal workings) are required to reach *explainability*. Several definitions for *interpretability* exist. Some refer to it as the ability to explain technology in human-understandable terms [22, 27], which in turn brings forth the question of what understandable means. Ras et al. [28], on the other hand, define interpretability as the extent to which “*a user is able to obtain true insights into how actionable outcomes are obtained*” and split the concept into the subproperties *clarity* and *parsimony* [28, p. 6]. High *clarity* is achieved when the explanation is unambiguous, while high *parsimony* is given when the user perceives it as simple, which depends on their capabilities. *Fidelity* generally describes whether an explanation is accurate. Kulesza et al. [29] divide fidelity further into *soundness* and *completeness*, where *soundness* describes whether the explanation is correct and faithful to the task model, and *completeness* is achieved when the explanation covers the entire dynamic of the task model.

¹Online: <https://www.mturk.com> [accessed: January 10, 2025]

ML explainability supports the social acceptance of, trust in, and social interaction with ML systems and fosters their safety and knowledge acquisition [10]. That is, the systems' safety may be increased through increasing its explainability [25], and so is the possibility for identifying faulty behavior, as more explainable systems may ease testing, auditing, and debugging [30]. Furthermore, explainability helps people to successfully interact with ML systems and eventually reach intended goals [30]. In short, ML explainability supports researchers and practitioners alike and, at the same time, helps extract the 'knowledge' a system uses [30]. Finally, the European Union's *Right to Explanation* [31] demonstrates the regulatory importance of humanly explainable ML systems, aiming to achieve equality and unbiased decision-making by algorithms [26]. Cheng et al. [32] support these efforts by defining the concept of *Socially Responsible AI Algorithms* and providing four fundamental responsibilities: functional, legal, ethical, and philanthropic.

2.2 Methods of CNN Explainability

Guidotti et al. [33] describe the *black-box explanation problem* as the challenge to provide an explanation of the black-box model through an interpretable system or method. The difficulty lies in providing insights about the internal processes that lead to a DNN's prediction and further clarifying under which circumstances they can be trusted [28] and producing insights into model predictions [34]. DNNs may have millions of parameters, making it hard to analyze their internal representations and the respective information flow throughout the network. Their complex learning procedure is determined by many components, including regularization, activation, and loss functions. Specifically, CNNs entail complex internal relations due to their structure. They consist of sequences of convolutional and pooling layers that learn increasingly higher-level features. The challenge here is to reduce the complexity of these operations, which is usually done by visualizing saliency maps [26]. In theory, it should be easier for humans to understand CNNs than regular DNNs that do not make use of convolutional layers, as our cognitive skills favor the understanding of this type of visual data [12]. This assumption has led to the definition of model-agnostic [35, 10] as well as model-specific methods, both of which aim to help with explanations for CNN decisions. Model-agnostic methods are applicable to any ML algorithm and are usually applied after the model has been trained – post-hoc [36]. While these methods analyze pairs of feature input and output, they do not have access to the inner information of the analyzed models [27]. Common methods in use are Local Interpretable Model-Agnostic Explanations (LIME) [10] and Shapley Values (SHAP) [35]. Model-specific methods either map the output back to the given input or explain the representation of the external world inside the layers [12, 26]. Most of the model-specific methods fall into the first category. Perturbation-based methods deliver good estimates of the input pixels' impact yet induce high computational costs [37]. Hence, backpropagation-based methods are commonly used, e.g., [38, 39, 40], as they compute the attributions with one or few forward and backward passes resulting in less computational costs [37]. Most backpropagation-based techniques achieve a balance in visualizing areas of high network sensitivity and high network activation [26]. One of the most prominent approaches here is Gradient-Weighted Class Activation Mapping (Grad-CAM) proposed by Selvaraju et al. [41]. Grad-CAM uses Class Activation Mapping (CAM), originally proposed by Zhou et al. [42], and visualizes the regions of an input image that are important for the model's prediction by using the class-specific gradient information. Further, this method applies to any CNN-based architecture and does not alter the architecture in any way.

2.3 Evaluating Explainability

Evaluating ML explainability has a two-fold goal [43]: First, it assesses if explainability is achieved. Here, the focus of the evaluation lies in determining whether the provided explainability method achieves the defined objective [23]. Second, it aims to formally compare available explainability methods and consequently identify preferences. One of the biggest challenges therefore lies in the evaluation itself, as no ground truth is given [44, 34]. This is especially true for post-hoc explainability methods, where one attempts to explain the inner workings of a black-box model. Finally, the ultimate target is to assess to what extent all properties of explainability are satisfied [43].

There are generally two factors that determine whether an ML model is understandable [45], i.e., the human's understanding given through capacity, and the model's features. Evaluating explainability is thus a result of combining these two factors. To this end, Doshi-Velez and Kim [22] describe three categories of explainability evaluation approaches.

Application-grounded evaluation measures the quality of an explanation in the context of its intended task, such as whether it results in less discrimination or better error identification. The benefit lies in testing to what extent the explainability method is helpful to the user [34]. Exemplary experiments include domain expert experiments with identical or simpler application tasks. For instance, if the task is to diagnose a particular disease, the most ideal way to demonstrate the model's workings is to have doctors perform the diagnosis. A good indication of explainability is how well they explain a decision [22].

The human-grounded evaluation assesses simpler human-subject experiments while maintaining the essence of the target application. This has several benefits, especially when the goal is to test general notions of explanation quality. Also, it is less expensive and may use a larger subject pool, as participants do not require domain expertise. Possible experiments include a binary forced choice, forward simulation, and counterfactual simulation. For instance, one might ask a user to simply choose the best fitting explanation from a pool of explanations [22].

Functionally-grounded evaluation does not demand human experiments but instead uses a formal definition of explainability as a proxy for explanation quality. Hence, it is most appropriate when a class of methods has already been evaluated, when a method is not yet mature enough, or when human-subject experiments would be unethical. The approach benefits from lower time and cost requirements, as no human-subject experiments are necessary [22]. However, Carvalho et al. [36] argue that results from a functionally-grounded approach have low validity, as human feedback is missing and the defined proxies may not fully measure explainability.

2.4 Evaluation Metrics

With application- and human-grounded evaluations, selecting the correct evaluation metrics plays a critical role in correctly evaluating a method. To this end, [45] differentiate between *subjective* and *objective* metrics. Subjective metrics are surveyed during, or after a task to gather the user's subjective response. They include trust, confidence, preference, or reasonability, and as such have been used in a variety of previous evaluations (e.g., [10, 46, 40]). Objective metrics are surveyed before, during, or after a task. They include human metrics, such as physiological and behavioral indicators, informed decision-making, task time length, or task performance. For instance, Schmidt and Biessmann [47] demonstrate that faster and more accurate decisions regularly indicate an intuitive understanding of explanations.

Functionally-grounded evaluation metrics, on the other hand, consist of various quantitative metrics to objectively assess the quality of an explanation, or more specifically whether certain explainability axioms are met [45]. Benchmarks without human intervention also fall under this category [34]. Examples contain model size [33], remove and retrain (ROAR) [48], diversity [49], sanity checks [17], or interaction strength [43].

While many quantitative metrics are proposed, a general computational benchmark across all possible explainability methods is difficult [49], as explainability is still a subjective concept where the perceived quality is user- and task-dependent.

2.5 Neural Network Pruning

Algorithm 1

Generic pruning algorithm

Require: N : number of iterations; x : data set
 Initialize W
 Train $f(x; W)$ to convergence
 Set M to ones
for i in N **do**
 Prune M according to selection criterion
 Fine-tune model $f(x; W)$ to convergence
end for
Ensure: M : pruning mask; W : fine-tuned model weights

NN pruning describes the reduction of network parameters to decrease the computational requirements and enhance the energy efficiency in constrained environments such as mobile or IoT devices [50] or for large foundational models [51]. Modern NNs are typically over-parameterized for the task at hand, leading to extensive redundancies in the model [52, 53]. The goal of pruning is to reduce these redundancies and memory requirements, which ultimately helps save computational resources. While the idea of network pruning was initially introduced in the late 1980s [54], it is the emergence of deep learning and the consequent rise in memory and storage requirements [55], which has recently led to increased interest in the concept. Moreover, it has been shown that a careful selection of the to-be-removed parameters does not only reduce the resource requirements of a model, but may even increase its accuracy [56, 57], robustness against adversarial attacks [58], and energy efficiency [50]. Research has shown that using NNs with a lower number of parameters from the start achieves lower accuracy values than using a larger model and pruning it retrospectively [57]. Furthermore, pruning can also be combined with other methods such as knowledge distillation, to increase the amount of compression without breaking convergence [59]. Pruning approaches may be described along five dimensions:

(1) The **selection criterion** defines how to select the parameters to be pruned. Many approaches have been proposed, e.g., magnitude-based (on absolute values) [57], based on the gradients [55], the Hessian matrix of the loss function [54], or based on the L_2 norm of the network structure [60]. Network pruning can also be incorporated into the DNN’s learning procedure [61] or be formulated as its own optimization problem [62]. Finally, random pruning often serves as a baseline and sanity check [55, 56].

(2) The **scope** determines whether the selection process is performed locally [60], where each layer is pruned separately, or globally, where all weights are considered simultaneously for the selection process. Global network pruning results in different sparsity levels in each layer, while local pruning yields a steady pruning ratio over the whole network [55].

(3) **Scheduling** defines when pruning is conducted. Most methods, e.g., [57], apply pruning after the training. The network is either pruned in one step to the desired compression rate [52], called one-shot pruning, or an iterative process of pruning and consequent training is applied [57, 63].

(4) The **pruning-structure** describes the granularity of a method, where the unstructured approach prunes single weights [54, 55], while structured pruning removes entire parts, such as kernels and filters [60], or even whole residual blocks [61]. Since the first approach produces sparse matrices of the same size as the unpruned network, dedicated hardware is necessary to accomplish practical improvements.

(5) **Fine tuning** refers to the training phase, which happens after pruning is applied. Here, recent work explores whether retraining a pruned network from scratch, using a new set of randomly initialized values, would lead to a different accuracy [52] than fine-tuning the remaining weights with their pre-pruning values [57]. To this end, the lottery ticket hypothesis proposed by Frankle and Carbin [56] suggests that a pruned network can reach a higher accuracy than its unpruned equivalent when retrained from scratch using its initial (random) values.

The number of parameters that are removed by NN pruning is determined by the compression rate, where a CR of 1 stands for the unpruned NN, while a CR of 2 yields a NN with only half of the original parameters, a CR of 4 that the resulting NN has only a fourth of the original NN’s parameters and so forth.

While other variations do exist, Algorithm 1 covers most pruning methods [55]. The procedure starts with an untrained model $f(x; W_0)$ and returns a pruned model $f(x; M \odot W')$ that has been fit to the training data x . W represents the model’s weights with $M \in \{0, 1\}^{|W'|}$ being a binary mask with the exact shape of W . By setting a value in $M_{i,k}$ to zero, its correspondent weight $W_{i,k}$ is effectively pruned as its value is always zero after the element-wise multiplication of W and M . Equally, the weight’s gradient is always zero, preventing it from taking on a non-zero value in the following learning iterations.

2.6 Neural Network Pruning to Increase Explainability

Previous work on leveraging NN pruning for ML explainability is scarce. Khakzar et al. [14] argue that current gradient-based attribution methods produce noisy results due to the complexity of current model architectures. Yet, if one uses input-specific pruning, where only neurons with high predictive contributions are kept, the global importance information of the attribution method may be improved. Their approach, called PruneGrad, differs from traditional model pruning in (1) that it does not take the whole dataset into account, (2) that it does not decrease the memory footprint, and (3) that it does not increase the inference speed. It is shown that roughly 50% of neurons can be removed without any changes in the output, while excessive pruning (i.e., over 80%) also removes highly contributing neurons and thus results in significant output changes. To perform a functionally-grounded evaluation of their PruneGrad method, Khakzar et al. [14] apply the sanity checks by Adebayo et al. [17], the pixel perturbation benchmark by Samek et al. [64], and the ROAR framework by Hooker et al. [48]. Evaluation results consistently outperform other gradient-based attribution methods.

On the other hand, Abbasi-Asl and Yu [65] extend previously proposed filter importance indices to visually apply filter pruning. Their structured algorithm prunes filters with visually redundant pattern selectivity, thereby increasing the explainability of the CNN. As a result, memory savings and smaller computational costs are reached while making the CNNs more explainable.

Other scientific contributions leverage explainability methods as a means for model pruning. For example, the work of Dotter and Ward [66] explores the suitability of datasets for certain models once they are pruned. Doing so, they show that visualizing a sample dataset of the final convolutional layer for different pruning ratios helps in making class separability visually understandable. Building on this, Zhang et al. [67] were the first to use explainability theory to guide channel pruning.

Other works apply different model explainability methods as CNN pruning criteria, as it is a challenge to identify criteria by which the importance of parameters can be measured. Yeom et al. [68] and Soroush et al. [69] use Layer-

wise relevance propagation (LRP) [70]. Their results show that the novel LRP criterion is not only comparable to state-of-the-art but outperforms previous criteria in transfer-learning scenarios. Sabih et al. [71] utilize DeepLIFT [39] to obtain the importance of certain neurons for NN pruning and the quantification of NN weights. With this, they aim to address a broad range of pruning methods, including structured, unstructured, CNN filter, and neuron pruning. Yao et al. [72] propose an explainability-based filter pruning framework based on activation maximization [73]. By visualizing every filter with activation maximization, they find that over 50% of the filters contain either repetitive or no information, making them redundant or invalid. The filters are then pruned based on a filter similarity matrix, which measures color and texture similarities. Related to the exploitation of explainability approaches for pruning, Cheng et al. [51] call for the development of explainable pruning methods in their survey paper. First efforts in this direction include the work of Yu and Xiang [74] for vision transformer architectures or the method of Rajapaksha and Crespi [75] for large language models. Frankle and Bau [76] examine the interpretability, quantitatively measured with the network dissection technique [77], of the ResNet50 pruned with the lottery ticket procedure [56] and find that network pruning has no influence for moderate compression rates. Finally, Arazo et al. [78] propose an evaluation metric that combines a model’s explainability, measured by the computable infidelity metric [79] with its compression rate in order to optimize the two objectives simultaneously.

Summarizing, we may argue that NN explainability methods are far more utilized to guide NN pruning than NN pruning is utilized to support NN explainability, although previous work has shown that there is merit in the latter. Thus, the goal of our work is to focus on NN pruning for ML explainability and measure its suitability using human-grounded evaluation.

3 Methodology

The goal of our work is to investigate the influence of NN pruning on the explainability of CNNs. In particular, we focus on the compression rates (CRs, cf. Sec. 2.5) as a variable to indicate the extent of NN pruning and assess its effects on perceived CNN explainability. In this sense, our methodology may be described as a three-phase experimental study, i.e., pre-study, Experiment 1, and Experiment 2. Following, we first describe the technical setup we used and then provide more details on the three human-grounded experiments.

3.1 Technical Setup

This section presents the technical details of the chosen model, dataset, pruning approach, and explainability method, along with the rationale for these selections.

3.1.1 Dataset and CNN Architecture



Figure 3: Example images of the Imagenette dataset with their labels.

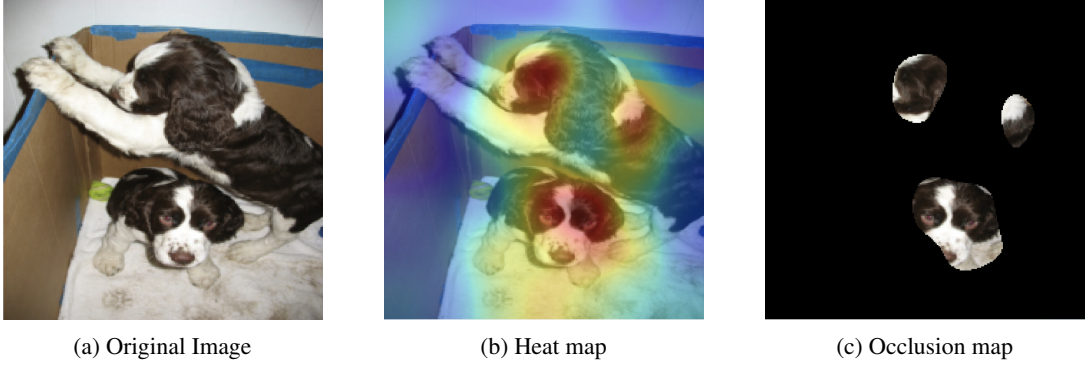


Figure 4: An image of the class 'dog', its heat- and occlusion map based on Grad-CAM and our calculations

We choose the Imagenette² dataset by FastAI for all experiments. Imagenette is a subset of Imagenet [80], one of the largest image databases for model benchmarks and research, and consists of ten classes, namely *tench, English springer, cassette player, chain saw, church, French horn, garbage truck, gas pump, golf ball, and parachute* [81]. Figure 3 shows one sample of each class in the dataset. The smaller size of the dataset requires fewer computational resources while still allowing the usage of models pre-trained on Imagenet as they share a similar data distribution. For the experiments, the class *tench* was changed to *fish*, and the class *English springer* was changed to *dog*. These changes simplify the Imagenette classes, as we could not anticipate our participants to have knowledge about fish species or dog breeds.

We employ the VGG-16 (configuration *D*) model proposed by Simonyan and Zisserman [82]. Its structure is simple and homogeneous, consisting of 13 convolutional layers and 3 fully connected layers. Due to its depth and high number of parameters (138 million) VGG-16 provides an adequate architecture for applying NN pruning. We initialize the model with pre-trained weights and fine-tune the model on Imagenette, resulting in a training accuracy of 99%, a validation accuracy of 98%, and a top-1 accuracy of 97% on the testset.

3.1.2 Pruning Approach

Following common baseline conventions in NN pruning research (e.g., [57], [63]), we use iterative magnitude-based weight pruning. According to the five dimensions introduced in Sec. 2.5, this means, for the *selection criterion* we chose the absolute values of the parameters, for the *scope* we opt for local, i.e., layer-wise pruning, for the *scheduling*, we follow the iterative paradigm, our *pruning-structure* is unstructured, and for *fine tuning*, we retrain every pruned model, for every CR {2, 4, 8, 16, 32}, after the pruning is completed until convergence, using the remaining weights with their pre-pruning values. Although other choices are possible, magnitude-based pruning methods are a reliable choice as they are widely adopted in current research and have been proven to yield competitive results in comparison with more sophisticated approaches [55]. Furthermore, previous research [57] has shown that magnitude-based methods yield better results when conducted iteratively. Thus, we refrain from examining one-shot pruning and implement our pruning methods strictly with an iterative pruning schedule. To ensure reproducibility, we utilize the PyTorch pruning library [83]. Additionally, we implement an object-oriented structure that allows us to easily and safely prune the convolutional layers of our converged VGG-16.

Furthermore, as convolutional layers contribute most to the inference time of CNNs and thus, have the greatest potential for theoretical speed-ups [84], we only prune the convolutional layers of the network. Figure 2 (on page 3) shows the top-1 accuracy on the Imagenette test-set for every CR, including the accuracy of the unpruned VGG-16 (= CR 1) (in dark blue).

3.1.3 Explainability Method

As mentioned in Sec. 2.2, backpropagation-based techniques visualize areas of high network sensitivity and high network activation [26], while only requiring one or few forward and backward passes [37]. Thus, we opt for the Grad-CAM approach due to its objective qualification as an explainability-method [17] and its relevance in both research and real-world applications.

Gradient-weighted Class Activation Mapping (Grad-CAM), proposed by Selvaraju et al. [16], is one of the most prominent backpropagation-based attribution methods. Grad-CAM applies post-hoc to any CNN-based architecture and

²Online: <https://github.com/fastai/imagenette> [accessed: January 10, 2025]

enables class-discriminative visualization. As shown by Mahendran and Vedaldi [85] and Bengio et al. [86], very deep convolutional layers capture instance-specific information and different types of image structures. Spatial information is then lost in the following fully connected layers. Therefore, deep convolutional layers represent the best option to capture higher-level semantics and spatial information. Grad-CAM aims to capture these high-level semantics and detailed spatial information from the network in order to identify image parts that were important for the classification decision. Similar to CAM, Grad-CAM uses the feature maps of the last convolutional layer. To calculate the Grad-Cam heat map, first, the gradient of the score for the respective image class y^c is calculated with respect to the activation map (outputs) A of the chosen target convolutional layer (commonly the last convolutional layer), i.e., $\frac{\partial y^c}{\partial A_{ij}^k}$. Global average pooling then yields a vector α_k^c with a weight for each channel of the activation map.

$$\alpha_k^c = \underbrace{\frac{1}{Z} \sum_i \sum_j}_{\text{global average pooling}} \frac{\partial y^c}{\partial A_{ij}^k}$$

Next, the activation map A^k is multiplied with the weight vector α_k^c and all channels are summed up, producing a heat map with the same height and width as the convolutional layer output. Finally, a *ReLU* operation is performed, canceling out all below-zero values. Similar to CAM, also Grad-CAM up-samples and normalizes the resulting heat maps for visualization.

$$L_{\text{GradCAM}}^c = \text{ReLU} \left(\sum_k \alpha_k^c A^k \right)$$

We implement Grad-CAM, utilizing the PyTorch hooking mechanisms and craft two types of images from the resulting activation-map matrices: Heat maps and occlusion maps. Figure 4 includes an example image with its heat map and occlusion map. For the **heat map** images, the activation-map matrix is up-sampled to the input image size of (224×224) pixels and visualized in colors from red (very important) to blue (least important). We then apply the heat map over the original image with an opacity of $\alpha = 0.4$. For the **occlusion map** images, the activation-map matrix is up-sampled to the input image size. Instead of colors indicating the importance, the least important 90% of the pixels are masked. These occlusion maps are inspired by the visualizations in Grad-CAM++[87], where the idea is to display only the parts of the image that appear to be most important to the network’s decision. After visual inspection of some examples with varying degrees of occlusion, we employ an occlusion rate of 90%.

3.2 Experimental Setup

Our research design is based on a three-phase approach, containing a pre-study and two more focused experiments. While the pre-study and the first experiment explore the participants’ subjective perception, the second experiment evaluates the participants’ performance based on objective metrics, leveraging Schmidt and Biessmann [47] findings that more accurate decision-making indicates better explanation.

We used Amazon’s Mechanical Turk¹ (MTurk) platform for all experiments to gather sufficient data. To ensure high-quality results, only MTurk respondents with a human intelligence task approval rate greater than 90% were admitted.

In the following, we present the setups for each of these phases and rationalize their design choices.

3.2.1 Pre-study

For the pre-study, we create heat- and occlusion maps for the models with CR 1, 2, and 32. CR 1, i.e., the non-pruned model, acts as the baseline. The great distance between CR 2 and CR 32 provided results from two different ends of the pruning spectrum. We use 500 Imagenette test-set images – 50 of each class. All test-set images are predicted correctly by all three models. For every image and CR, we created a heat- and an occlusion map, resulting in three heat maps and three occlusion maps per image, i.e., a total of 1 500 heat maps and 1 500 occlusion maps. Participants were confronted with three images:

1. the original image, always placed in the middle with the correctly predicted class,
2. a heat map image crafted with the unpruned model, randomly placed on either the left or right side, and
3. a heat map image crafted by either the CR 2 model or the CR 32 model on the other side.

The setup generates a total of 1 000 unique tasks (two for each original image). The CR is unknown to the participants, assuring a blind study setup. Participants were asked to select the algorithm whose predictions they believed were

cmr	smr	eq	slr	clr	standard deviation
[+2, -2]					
[0, 0]	0	0	0	5]	0
[0, 0]	0	0	1,	4]	0.4
[0, 1]	1	1,	2,	1]	1.0198
[0, 1]	1	1,	1,	2]	1.1662
[1, 1]	1	1,	1,	1]	$\sqrt{2}$
[1, 1]	1	0,	2,	1]	1.4697
[2, 0]	0	0,	0,	3]	1.9596

Table 1: Examples of inter-rater agreement and the corresponding standard deviations.

more reasonable, or in case both algorithms felt equally reasonable select the middle point, effectively representing a three-point Likert scale. We have deliberately chosen the less-technical term 'reasonable' as initial tests have shown that participants had a better understanding of this term than 'explainable'. The same setup was used for the occlusion map images, resulting in another 1 000 unique tasks. Exemplary setups of the pre-study can be found in Figures 12 and 13 in Appendix A. Each of the 2 000 unique tasks was answered five times, generating a total of 10 000 answers.

3.2.2 Experiment 1

Lessons learned from our pre-study, that influenced the setup of Experiment 1 were: First, the CRs do influence the explainability of the CNN, second, heat maps seem to be more suitable than occlusion maps for the evaluation with a subjective metric, and third, CR 32 has a negative impact on the accuracy (cf. Figure 2, on page 3) and the explainability to humans³. With these lessons in mind, we use heat maps only for Experiment 1. Furthermore, we extend the three-point Likert scale to a five-point Likert scale and disregard the model with CR 32 in favor of models with CR 4 and CR 8. Figure 1 (on page 2) shows the presentation of a single task. For this experiment, we focus on the heat map images, as the pre-study has shown that these images produce clearer results. Again, participants were asked to decide which of the algorithms was more reasonable in its decision-making based on the shown heat map images. This time, participants were asked to make a more nuanced selection based on a 5-point Likert scale running from *clearly more reasonable* (cmr) to *clearly less reasonable* (clr) with *slightly more reasonable* (smr), *equally reasonable* (eq), and *slightly less reasonable* (slr) in between. We crafted 500 heat map images for the CRs 1, 2, 4, 8, and compared each CR with every other CR, resulting in 3 000 unique tasks. Every unique task was answered by 5 respondents, generating a total of 15 000 answers.

Evaluation

To calculate inter-coder agreement, we encode all answer possibilities with values ranging from -2 for *clearly less reasonable* to +2 for *clearly more reasonable*. We then calculate Krippendorff's α [88] to evaluate the agreement level.

Additionally, we report the inter-rater agreement based on the standard deviation of the respondents per task. With five respondents per task and the answers encoded as mentioned above, the standard deviation may compute to 26 different values ranging from 0 (where we have full agreement, i.e., all respondents choose the same option) to 1.9596 (where we have complete disagreement, e.g., two respondents answer with clearly more reasonable and three with clearly less reasonable or the other way around). Thus, we can say that lower values indicate more agreement among respondents, while higher values translate to more disagreement. The value of $\sqrt{2}$ (i.e., one answer per option) may serve as a baseline that indicates randomness, meaning that values below $\sqrt{2}$ tend to represent more agreement and values above more disagreement. To give an intuition we sampled some of these 26 possibilities in Table 1.

As we cannot assume explainability to be transitive (i.e., even if the CR 2 model produces more reasonable heat maps than the CR 1 model and the CR 4 model produces more reasonable heat maps than the CR 2 model, we cannot be sure that the CR 4 model is more reasonable than the CR 1 model), we observe all tasks that contain a specific CR. Exemplary for CR 1, we accumulate all tasks that compare CR 1 with either CR 2, CR 4, or CR 8. The mean of all respondents' answers, encoded as above, creates a metric that describes the explainability of this specific model relative to all other examined models. We define this number as a model's *explainability index* which allows for a direct comparison between all algorithms. A higher value indicates superior explainability compared to the remaining algorithms.

³We report detailed results of the pre-study in Section 4.1.

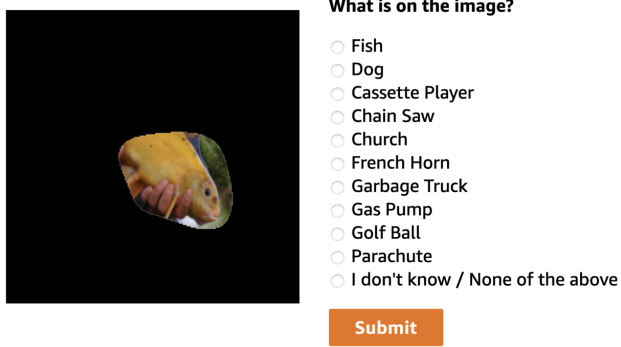


Figure 5: Experimental Setup - Experiment 2: occlusion map (CR 1).

	CR 1 vs CR 2 (more reasonable in %*)	CR 1 vs CR 32 (more reasonable in %*)
heat maps	46.6% vs 53.4%	52.9% vs 47.1%
occlusion maps	45.0% vs 55.0%	54.2% vs 45.8%
	<i>equally reasonable in %</i>	<i>equally reasonable in %</i>
heat maps	38.68%	13.16%
occlusion maps	53.72%	26.40%

* % based on answers without “equal reasonability”

Table 2: Explainability comparison of pre-study results for different CRs and visualization methods.

3.2.3 Experiment 2

Experiment 2 aims to assess the effects of different CRs on Grad-CAM occlusion maps and how they differ from human-understandable areas. Participants were confronted with a single occlusion map, crafted as described in Section 3.1, i.e., based on models with CR 1, 2, 4, 8, and 32. All occlusion maps appear in random order to prevent the occlusion map of an identical image. Next to the occlusion map, all ten Imagenette classes are listed as possible answers, as depicted in Figure 5. The respondents were instructed to choose the most suitable class for the map. In case they felt that none of the classes would fit, they were asked to choose ‘I don’t know / None of the above’. The accuracy of the respondents’ answers provides an objective evaluation metric. Note that this setup relies on occlusion instead of heat maps as participants would be able to see the whole image and thus know exactly what the image displays. In total, this results in 2 500 unique tasks, as 5 occlusion maps of 500 images were crafted - one for every CR. Every unique task was answered five times, generating a total of 7 500 answers.

Evaluation

To assess the inter-rater agreement we calculate Krippendorff’s α [88]. As for this experiment, a clear ground truth is available we are able to calculate the human-observer accuracy as the ratio of correct answers and the total amount of answers. Additionally, we report the error rate as the ratio between wrong answers and the total number of answers as well as the ratio of images for which the respondents are indecisive. We report these numbers for each CR in $\{1, 2, 4, 8, 32\}$ over all classes and for each individual class.

4 Results

Following we elaborate on the results of our three studies and reflect on their findings.

4.1 Pre-study

Investigating agreement levels, the pre-study setup with heat maps achieves a Krippendorff’s α score of 0.13, while the setup with occlusion maps achieves a score of 0.24. This indicates a rather low agreement across respondents as to which CR for particular images appears more reasonable. The higher value for the occlusion maps stems from the fact that here more respondents believe that both models seem equally reasonable.

	total	CR 1	CR 2	CR 4	CR 8
Krippendorff's α	0.086	0.0916	0.0777	0.0913	0.0904
mean over standard deviations	1.0036	0.9904	0.9784	1.0034	1.0424
	CR 1 vs. CR 2	CR 1 vs. CR 4	CR 1 vs. CR 8	CR 2 vs. CR 4	CR 2 vs. CR 8
Krippendorff's α	0.049	0.1168	0.0985	0.0806	0.0962
mean over standard deviations	0.8873	1.0185	1.0654	0.9889	1.0588
	CR 4 vs. CR 8				

Table 3: Inter-rater agreement for the first experiment. The “total” column is measured over all responses, the other four columns in the top row are calculated per CR against all other CRs, and all lower columns are calculated for the specified CR comparison.

Furthermore, we find that the three CRs used (1, 2, and 32) do make a difference in explainability. The upper half of Table 2 compares the percentages of explainability between heat- and occlusion maps. The results indicate that the unpruned model has worse explainability than the CR 2 model but is more explainable than the CR 32 model.

The lower half of Table 2 presents the percentage of respondents that chose “Both are equally reasonable”. We can see that this number is clearly higher for occlusion maps. A higher number for “equally reasonable” indicates that NN pruning does not have as much of an effect on the explainability of the occlusion maps.

Overall, Table 2 suggests that occlusion maps are more robust to different pruning ratios, as can be seen by the higher number of indecisive respondents, and thus not as suitable to assess the difference between different pruning ratios as heat maps. Hence, one of the most important results from our pre-study is that considering the task of assessing explainability to humans, heat maps are more suitable than occlusion maps.

4.2 Experiment 1: Which Algorithm is More Reasonable?

We report the inter-rater agreement for the first experiment in Table 3. Independent of the applied CR, Krippendorff's α is relatively low, indicating low agreement among the respondents. As described in Section 3.2.2, we further report the mean over the per-task standard deviation. Over all tasks, we observe values between 0 (complete agreement) and 1.9596 (complete disagreement). Further, the mean of the standard deviation over all tasks is 1.0036, which is clearly below $\sqrt{2}$ (the standard deviation of a uniform distribution), indicating a certain level of agreement among the respondents.

Figure 6 depicts all per comparison results. The first three graphs show the accumulated answers for the comparisons of the unpruned model with models pruned with CR 2, 4, and 8, respectively. We observe that the proportion of participants rating both algorithms equally reasonable declines when increasing the CR. Further, the last three graphs in Figure 6 show the accumulated answers for the tasks in which two pruned models are compared. Apart from the change in the number of respondents that find both algorithms equally reasonable, visually no clear trends are detectable. However, in Table 4 we report the mean of the respective encoded answers. Values above 0 indicate that the first-mentioned algorithm produces more explainable heat maps while values below 0 indicate the opposite. One can see that in total, pruning with CRs 2, 4, and 8 (upper three lines) seems to help the explainability to human raters. Transitivity, however, is not given. When considering the baseline experiments comparing the unpruned with the pruned models, we would expect the CR 8 model to produce better explainable heat maps than the CR 2 model. However, when comparing the respective heat maps directly, participants perceived the heat maps of the CR 2 model to be more reasonable than both, the CR 4 and CR 8 model (as can be seen in lines 4 and 5 of Table 4).

Table 5 illustrates the explainability index as described in Section 3.2.2, that is the explainability of heat maps produced with every CR compared to every other CR. By this metric, measured over all tested images, heat maps produced with the CR 8 model explain the model's decision most reasonably. Interestingly, the CR 2 and the CR 4 models both produce more reasonable explanations than the unpruned model as the orange line in Figure 2 (on p. 3) indicates.

4.3 Experiment 2: What is on the Image?

We assess the inter-rater agreement for this experiment with Krippendorff's α . Table 6 shows the α -values over all answers and for the specific CRs. The overall α of 0.76 indicates a reasonably high agreement among the respondents. Interestingly, the inter-rater agreement is higher for the unpruned (≈ 0.80) and CR 2 pruned (≈ 0.79) models and declines for higher pruning ratios (≈ 0.74).

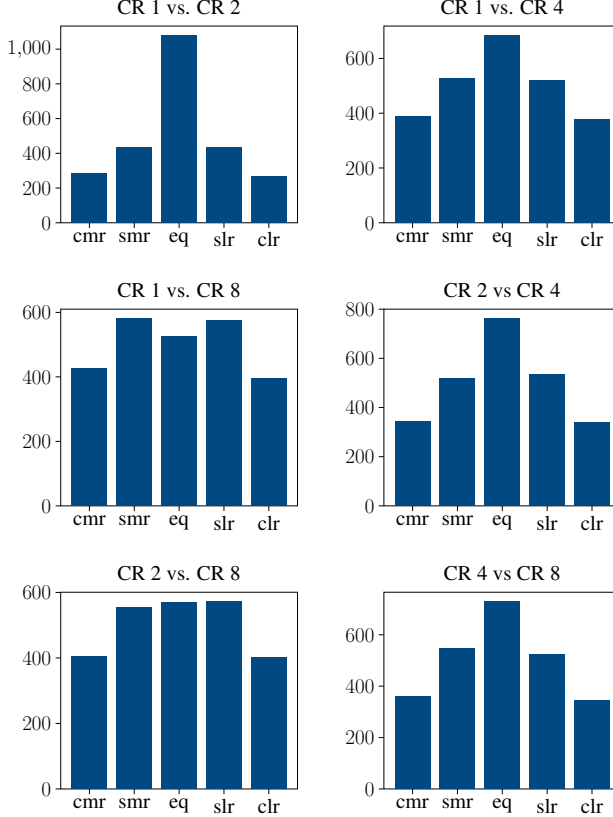


Figure 6: The distribution of participants' answers for each model comparison. The higher CR is always compared to the lower CR. (Mind the different y-axes.)

Algorithm 1	Algorithm 2	Mean
CR 1	CR 2	-0.0128
CR 1	CR 4	-0.0104
CR 1	CR 8	-0.0272
CR 2	CR 4	0.0036
CR 2	CR 8	0.0048
CR 4	CR 8	-0.0232

Table 4: Mean over all answers for the specific comparisons with answers encoded from -2 (Algorithm 1 is clearly less reasonable) to +2 (Algorithm 1 is clearly more reasonable).

Table 6 further shows the overall results of the second experiment. Mind that all values refer to the human-respondents' performance. We observe that the participants achieve a slightly higher accuracy for the occlusion maps produced with the CR 2 model (86.40%) over those produced with the unpruned model (85.84%). For higher pruning rates, the human-rater accuracy declined by 4.32% (CR 4) to 5.2% (CR 8). The human error rate is relatively stable, with the lowest value for the unpruned model (4.36%) and the highest values for CR 4 and CR 8 (5.36% each). For the ratio of answers in which the respondents have chosen the option 'I don't know / None of the above' we observe a marginal decline from CR 1 (9.8%) to CR 2 (8.96%) and a subsequent rise up to 14.2% for CR 32. Higher indecisiveness of the respondents indicates lower explainability due to indecipherable occlusion maps. However, indecisiveness might be preferable over a wrong answer since it would be better for an explanation map to explain nothing rather than explaining the wrong class. The light blue line in Figure 2 (on page 3) shows the human rater accuracy and Figure 7 illustrates the distribution of respondents' answers visually.

We find that the human-rater performance differs vastly between the classes. Table 7 displays the accuracies for all ten classes dependent on the CR of the used model. For occlusion maps produced with the unpruned model, human-rater accuracy ranges from 66% (chainsaw) to 95.6% (golfball). Interestingly, the impact of NN pruning on the explainability of the produced occlusion maps is also dependent on the class. For some classes, the human-rater accuracy declines

Algorithm	Explainability Index
CR 1	-0.0168
CR 2	0.0071
CR 4	-0.0055
CR 8	0.0152

Table 5: Explainability index for all models

	Accuracy	Error-rate	Indecisive	Krippendorff's α 's
CR 1	85.84%	4.36%	9.80%	0.799268
CR 2	86.40%	4.64%	8.96%	0.790250
CR 4	82.08%	5.36%	12.56%	0.744596
CR 8	81.20%	5.36%	13.44%	0.738209
CR 32	81.32%	4.48%	14.20%	0.744790

Table 6: Overall results and inter-rater agreement of Experiment 2.

sharply when the underlying model is pruned. As an example, the human-rater performance for the class ‘parachute’ is high (88%) with the unpruned model, but heavily declines for CR 2 (80.4%) and CR 4 (71.2%). On the other hand, for the class ‘dog’ respondents achieved the lowest accuracy (90%) for occlusion maps produced with the unpruned model, while they were able to correctly classify the occlusion maps produced with the CR 8 model in more than 97% of the cases. A similar observation can be made when looking at the ratio of occlusion maps for which the respondents choose the option ‘None of the above / I don’t know’. For the class ‘parachute’ the number of indecisive respondents almost doubled when comparing occlusion maps from the CR 1 (8.8%) and the CR 2 (16.0%) model and rises even over 20% for the CR 4, CR 8, and CR 32 model. Reversely, for the class ‘church’ indecisiveness was the highest for the CR 1 model (12.8%) while the CR 2 model produced the lowest value with 3.6%. These findings suggest that the images’ semantics impact the explainability of the models’ decisions. We include the full table for the respondents’ indecisiveness in Appendix C.

Error rates are relatively stable among the classes and the various models, as is visible in the right half of Table 7. Respondents misclassified occlusion maps of the class ‘chainsaw’ most often (11.6%) and pruning slightly increases the error rate. For the class ‘cassette player’, another class with a comparatively low human-rater accuracy (see Table 7) and a higher error rate of 7.2%, mild pruning (CR 2) decreases the error rate by 1.6% to 5.6%, while more extensive pruning increases the error rate to 10.8% (CR 4 and CR 8).

The specific errors between the classes are visualized with confusion matrices in Figure 8. We observe higher error rates for occlusion maps of images containing chainsaws and garbage trucks. This holds true for CR 1 and CR 2 and is also visible for higher CRs. We provide the respective confusion matrices in Appendix C. Figure 9 illustrates a case in which fewer misclassifications occurred for the occlusion map produced by the pruned model.

class	Human rater accuracies					Human rater error rates				
	CR 1	CR 2	CR 4	CR 8	CR 32	CR 1	CR 2	CR 4	CR 8	CR 32
fish	91.2%	92.4 %	84.0 %	77.6 %	76.4 %	2.0%	0.4 %	2.4%	4.0%	6.0%
dog	90.0%	95.2 %	95.6 %	97.2 %	96.0 %	1.2%	0.8 %	2.0%	0.8 %	0.8 %
cassette player	79.6%	82.4 %	73.2 %	71.6 %	77.6 %	7.2%	5.6 %	10.8%	10.8%	8.4%
chainsaw	66.0 %	66.0 %	58.8 %	56.4 %	52.4 %	11.6 %	12.0%	14.8%	14.4%	12.0%
church	85.2%	92.4 %	90.8 %	89.6 %	88.4 %	2.0%	4.0%	1.6%	0.8 %	1.6%
french horn	94.0 %	94.0 %	86.8 %	89.6 %	94.4 %	2.0%	2.8%	6.0%	4.4%	0.4 %
garbage truck	86.0%	88.0 %	86.4 %	84.8 %	84.4 %	6.8%	6.8%	6.0%	5.6%	3.6 %
gas pump	82.8 %	76.0 %	77.6 %	77.2 %	78.8 %	5.6 %	9.2%	8.0%	6.8%	8.4%
golfball	95.6%	97.2 %	96.4 %	91.6 %	88.0 %	2.0%	1.2%	0.8 %	2.4%	2.0%
parachute	88.0 %	80.4 %	71.2 %	76.4 %	76.8%	3.2%	3.6%	1.2 %	3.6%	1.6%
total	85.85%	86.40 %	82.08%	81.20 %	81.32 %	4.36 %	4.64%	5.36%	5.36%	4.48%

Table 7: Accuracies and error rates per class for human raters in Experiment 2. Maximum, resp. minimum are highlighted in boldface.

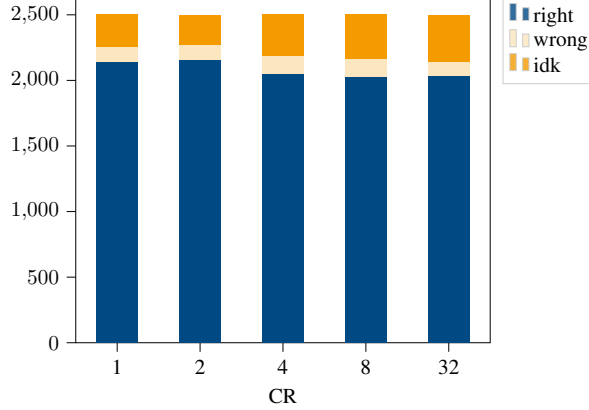


Figure 7: Respondents' answers in Experiment 2 for all CRs.

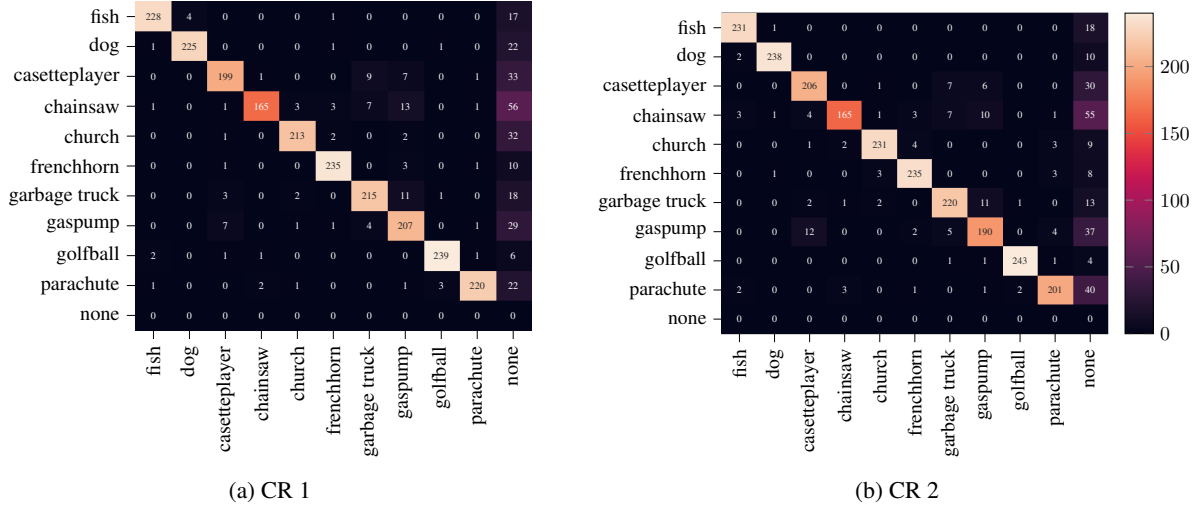


Figure 8: Confusion matrices of the human ratings from Experiment 2 for all ten classes and CRs 1 (Subfigure 8a) and 2 (Subfigure 8b). Darker values indicate lower numbers and lighter values indicate higher numbers. The diagonals display correct classifications, while the right-most column shows the number of 'I don't know / None of the above'. Confusion matrices of CR 4, 8, and 32 can be found in Appendix C.

5 Limitations

We measure only low reliability scores for Krippendorff's α for the pre-study and the first experiment. We believe that these scores are caused by the following: As pointed out in [18], the concept of explainability is subjective and domain-specific. Therefore, comparing the reasonability of two algorithms might be subjective to every respondent, especially when the two heat- or occlusion maps do not show significant differences. This may lead to different perceptions of the visualizations that differ among the respondents. It may further explain why the scores for Krippendorff's α are higher in the pre-study, where a three-point Likert scale was provided than in Experiment 1, where we provided a five-point Likert scale.

Looking at specific samples might help in understanding how complete agreement or complete disagreement might emerge. Subfigure 10a illustrates one example in which all respondents agree that algorithm 1 is more reasonable. While the right heat map highlights some parts on the right of the ball, the left heat map covers the whole ball. Both heat maps assign less importance to the print in the middle of the ball. Additionally, the heat map on the right highlights the tee more concisely. Conversely, Subfigure 10b illustrates the case of complete disagreement, i.e., three respondents chose algorithm 1 to be clearly more reasonable, and two respondents chose algorithm 2 to be clearly more reasonable. The model on the left seems to take more details into account. The participants' degree of familiarity with the subject might be an influencing factor regarding which algorithm appears to be more reasonable. The lack of a definite ground truth encountered in the first experiment highlights one of the most pressing issues within explainable AI research.

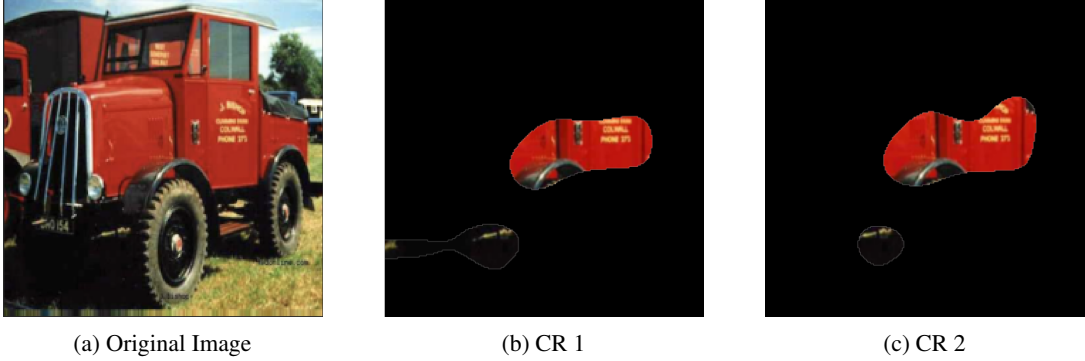


Figure 9: The original image and occlusion maps produced by the CR 1 and CR 2 models of the class ‘garbage truck’. 3/5 respondents misclassified the CR 1 occlusion maps as a gas pump, while 2/5 respondents misclassified the CR 2 model as a gas pump.

Müller and Holzinger [89] proposed the Kandinsky Patterns as a potential solution. These abstract patterns have easily extractable structures of geometric shapes that might allow an evaluation against a given ground truth.

In Experiment 2, we report a rather high reliability score. In comparison to the subjectiveness of perceived explainability, Experiment 2 proposes an objective measure with clear ground truth, as an image always includes one of the ten Imagenette classes. If the respondents were not able to recognize the image class, they had the chance to choose ‘I don’t know / None of the above’. Figure 11 shows the occlusion maps for all five CRs. For this sample, inter-rater agreement is reasonably high. Respondents who did not choose the correct answer all selected ‘I don’t know / None of the above’. Looking at the occlusion maps, we observe that the CR 1, CR 8, and CR 32 models base their prediction more on latent features of the image such as the pose of the human and the presence of a tree, while the CR 2 and particularly the CR 4 model base their decision on the object in question, a chainsaw, itself. Hence, it does not seem surprising that humans struggle to classify these samples correctly.

6 Future Work

Directions for future work, identified through our analysis, include the extension of the five-point Likert scale to a seven-point Likert scale and an experimental setup with more raters per task, maybe at the cost of a lower number of images. Carefully selecting these images, for example, by some kind of image complexity measure, would furthermore shed light on the open question about the relation between image complexity and explainability. Additionally, our setup is restricted to one explainability method and one pruning method, while there is a lot of ongoing work in each of these areas.

Besides these direct extensions of our experiments, there are several dimensions in which our work can be diversified to reach more reliable results, especially regarding generalizability. First and foremost, the generalization to other CNN architectures such as ResNets [90], Inception [91] or EfficientNets [92] should be examined. Given that we choose an explainability method that is applicable to all CNNs, the open question is not if our methodology is applicable but rather if the results obtained for VGG-16 in this work also hold for other CNN architectures, and subsequently also for the novel class of transformer-based computer vision architectures, such as Swin [93] and Vision Transformers [94]. The development of a unified evaluation metric for explainability and network compression as proposed by Yu and Xiang [74] is a promising direction to optimize both objectives simultaneously during the training process. Finally, it might be worthy to examine the impact of NN pruning on the internal mechanisms of GradCAM (e.g., in the used activation maps) and how these changes are reflected in our human-grounded experiment results. Exploring each of these dimensions is a valuable direction for future work and given that we carefully selected our setup, we are positive that similar setups will result in similar sweet spots.

7 Conclusion

Our results suggest that there exists a sweet spot of mild pruning, that helps explainability without hurting human decision accuracy. This might not come as a surprise as a lower number of (important) parameters seems to intuitively go along with higher explainability. But, our experiments also showed that for explainability research we always have to cover both, the subjective and the objective aspects. We did so by covering the subjective aspect in Experiment 1, which



(a) Heat maps produced with the CR 4 model on the left and the CR 8 model on the right. All participants marked algorithm 1 to be clearly more reasonable.



(b) Heat maps produced with the CR 4 model on the left and the unpruned model on the right. Three participants marked algorithm 1 as clearly more reasonable, while two participants marked algorithm 2 as clearly more reasonable.

Figure 10: Samples from Experiment 1 that yield complete agreement and complete disagreement among the human raters

indicates that a CR of 8 produces the best explanations. Taking the objective measure of human decision accuracy in Experiment 2 into account, however, we see that all CRs above 2 have a negative influence on the accuracy of the participants.

It is common knowledge in the machine learning community and can be seen in Figure 2 (on p. 3) that mild pruning also increases the accuracy of the underlying DNN [57]. Furthermore, turning to *adversarial machine learning*, which is concerned with the security of machine learning algorithms, we find evidence that mild pruning increases the robustness of the classifiers against malicious adversaries [58].

Combining our results on NN pruning and explainability with these results from machine learning and adversarial machine learning suggests that NN pruning might be a “jack of all trades”, decreasing complexity, computation time, and power consumption while simultaneously increasing explainability, accuracy, and security.

References

- [1] Justin Ker, Lipo Wang, Jai Rao, and Tchoyoson Lim. Deep learning applications in medical image analysis. *Ieee Access*, 6:9375–9389, 2017.
- [2] Christian Ploder, David Weber, Reinhard Bernsteiner, and Stephan Schlögl. Knowledge gain in production planning and execution systems. In Lorna Uden, I-Hsien Ting, and Kai Wang, editors, *Knowledge Management in Organizations*, pages 138–146, Cham, 2021. Springer International Publishing. ISBN 978-3-030-81635-3.
- [3] Mamoun Alazab and MingJian Tang. *Deep learning applications for cyber security*. Springer, 2019.

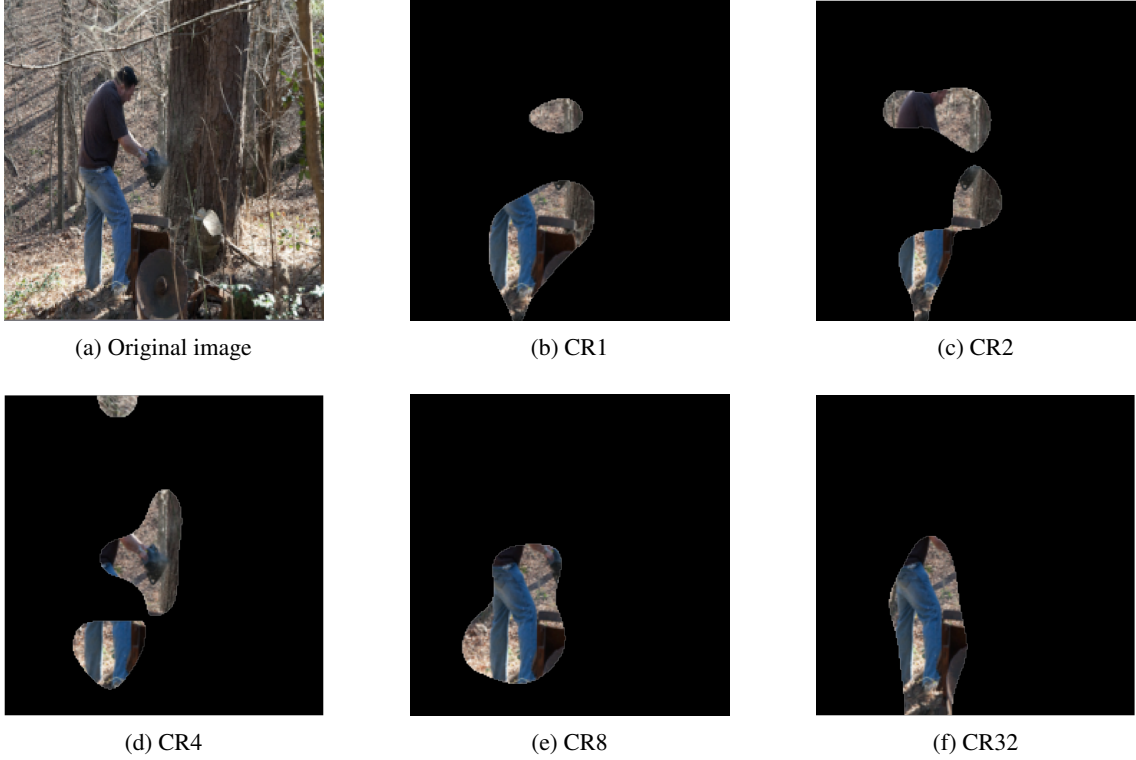


Figure 11: The original image and occlusion maps for one sample of the class chainsaw. Human rater accuracies are 1/5 for CR 1, 4/5 for CR 2, 5/5 for CR 4, and 0/5 for CR 8 and CR 32.

- [4] Jian Huang, Junyi Chai, and Stella Cho. Deep learning in finance and banking: A literature review and classification. *Frontiers of Business Research in China*, 14:1–24, 2020.
- [5] Soumava Dey, Gunther Correia Bacellar, Mallikarjuna Basappa Chandrappa, and Raj Kulkarni. Covid-19 chest x-ray image classification using deep learning. *medRxiv*, , 2021.
- [6] Hafsa Moontari Ali, M Shamim Kaiser, and Mufti Mahmud. Application of convolutional neural network in segmenting brain regions from mri data. In *International Conference on Brain Informatics*, pages 136–146. Springer, 2019.
- [7] Ajeet Ram Pathak, Manjusha Pandey, and Siddharth Rautaray. Application of deep learning for object detection. *Procedia computer science*, 132:1706–1717, 2018.
- [8] Xu Han, Zhengyan Zhang, Ning Ding, Yuxian Gu, Xiao Liu, Yuqi Huo, Jiezhong Qiu, Yuan Yao, Ao Zhang, Liang Zhang, et al. Pre-trained models: Past, present and future. *AI Open*, 2:225–250, 2021.
- [9] Gurusha Lulla, Abhinav Kumar, Govind Pole, and Gopal Deshmukh. Iot based smart security and surveillance system. In *2021 international conference on emerging smart computing and informatics (ESCI)*, pages 385–390. IEEE, 2021.
- [10] Marco Tulio Ribeiro, Sameer Singh, and Carlos Guestrin. " why should i trust you?" explaining the predictions of any classifier. In *Proceedings of the 22nd ACM SIGKDD international conference on knowledge discovery and data mining*, pages 1135–1144, 2016.
- [11] Mengnan Du, Ninghao Liu, and Xia Hu. Techniques for interpretable machine learning. *Communications of the ACM*, 63(1):68–77, 2019.
- [12] Alejandro Barredo Arrieta, Natalia Díaz-Rodríguez, Javier Del Ser, Adrien Bennetot, Siham Tabik, Alberto Barbado, Salvador García, Sergio Gil-López, Daniel Molina, Richard Benjamins, et al. Explainable artificial intelligence (xai): Concepts, taxonomies, opportunities and challenges toward responsible ai. *Information Fusion*, 58:82–115, 2020.
- [13] Nadia Burkart and Marco F Huber. A survey on the explainability of supervised machine learning. *Journal of Artificial Intelligence Research*, 70:245–317, 2021.

[14] Ashkan Khakzar, Soroosh Baselizadeh, Saurabh Khanduja, Christian Rupprecht, Seong Tae Kim, and Nassir Navab. Improving feature attribution through input-specific network pruning. *arXiv preprint arXiv:1911.11081*, , 2019.

[15] Karen Simonyan, Andrea Vedaldi, and Andrew Zisserman. Deep inside convolutional networks: Visualising image classification models and saliency maps. In Yoshua Bengio and Yann LeCun, editors, *2nd International Conference on Learning Representations, ICLR*, 2014.

[16] Ramprasaath R Selvaraju, Michael Cogswell, Abhishek Das, Ramakrishna Vedantam, Devi Parikh, and Dhruv Batra. Grad-CAM: Visual Explanations from Deep Networks via Gradient-Based Localization. *International Journal of Computer Vision*, 128(2):336–359, 2020. ISSN 1573-1405. doi:10.1007/s11263-019-01228-7. URL <https://doi.org/10.1007/s11263-019-01228-7>.

[17] Julius Adebayo, Justin Gilmer, Michael Muelly, Ian Goodfellow, Moritz Hardt, and Been Kim. Sanity checks for saliency maps. *arXiv preprint arXiv:1810.03292*, , 2018.

[18] Cynthia Rudin. Please stop explaining black box models for high stakes decisions. *stat*, 1050:26, 2018.

[19] Plamen Angelov and Eduardo Soares. Towards explainable deep neural networks (xdnn). *Neural Networks*, 130: 185–194, 2020.

[20] Erico Tjoa and Cuntai Guan. A survey on explainable artificial intelligence (xai): Toward medical xai. *IEEE Transactions on Neural Networks and Learning Systems*, , 2020.

[21] Amina Adadi and Mohammed Berrada. Peeking inside the black-box: a survey on explainable artificial intelligence (xai). *IEEE access*, 6:52138–52160, 2018.

[22] Finale Doshi-Velez and Been Kim. Towards a rigorous science of interpretable machine learning. *arXiv preprint arXiv:1702.08608*, , 2017.

[23] Zachary C Lipton. The mythos of model interpretability: In machine learning, the concept of interpretability is both important and slippery. *Queue*, 16(3):31–57, 2018.

[24] Federico Cabitza, Andrea Campagner, and Davide Ciucci. New frontiers in explainable ai: understanding the gi to interpret the go. In *International Cross-Domain Conference for Machine Learning and Knowledge Extraction*, pages 27–47. Springer, 2019.

[25] Tim Miller. Explanation in artificial intelligence: Insights from the social sciences. *Artificial intelligence*, 267: 1–38, 2019.

[26] Leilani H Gilpin, David Bau, Ben Z Yuan, Ayesha Bajwa, Michael Specter, and Lalana Kagal. Explaining explanations: An overview of interpretability of machine learning. In *2018 IEEE 5th International Conference on data science and advanced analytics (DSAA)*, pages 80–89. IEEE, 2018.

[27] Christoph Molnar, Giuseppe Casalicchio, and Bernd Bischl. Interpretable machine learning—a brief history, state-of-the-art and challenges. In *Joint European Conference on Machine Learning and Knowledge Discovery in Databases*, pages 417–431. Springer, 2020.

[28] Gabriëlle Ras, Marcel van Gerven, and Pim Haselager. Explanation methods in deep learning: Users, values, concerns and challenges. In *Explainable and interpretable models in computer vision and machine learning*, pages 19–36. Springer, 2018.

[29] Todd Kulesza, Simone Stumpf, Margaret Burnett, Sherry Yang, Irwin Kwan, and Weng-Keen Wong. Too much, too little, or just right? ways explanations impact end users’ mental models. In *2013 IEEE Symposium on visual languages and human centric computing*, pages 3–10. IEEE, 2013.

[30] Christoph Molnar. *Interpretable Machine Learning*. 2 edition, 2022. URL <https://christophm.github.io/interpretable-ml-book>.

[31] Bryce Goodman and Seth Flaxman. European union regulations on algorithmic decision-making and a “right to explanation”. *AI magazine*, 38(3):50–57, 2017.

[32] Lu Cheng, Kush R Varshney, and Huan Liu. Socially responsible AI algorithms: Issues, purposes, and challenges. *Journal of Artificial Intelligence Research*, 71:1137–1181, 2021.

[33] Riccardo Guidotti, Anna Monreale, Salvatore Ruggieri, Franco Turini, Fosca Giannotti, and Dino Pedreschi. A survey of methods for explaining black box models. *ACM computing surveys (CSUR)*, 51(5):1–42, 2018.

[34] Gabrielle Ras, Ning Xie, Marcel van Gerven, and Derek Doran. Explainable deep learning: A field guide for the uninitiated. *Journal of Artificial Intelligence Research*, 73:329–397, 2022.

[35] Scott M Lundberg and Su-In Lee. A unified approach to interpreting model predictions. In *Proceedings of the 31st international conference on neural information processing systems*, pages 4768–4777, 2017.

[36] Diogo V Carvalho, Eduardo M Pereira, and Jaime S Cardoso. Machine learning interpretability: A survey on methods and metrics. *Electronics*, 8(8):832, 2019.

[37] Marco Ancona, Enea Ceolini, Cengiz Öztïreli, and Markus Gross. Towards better understanding of gradient-based attribution methods for deep neural networks. *arXiv preprint arXiv:1711.06104*, , 2017.

[38] Mukund Sundararajan, Ankur Taly, and Qiqi Yan. Axiomatic attribution for deep networks. In *International Conference on Machine Learning*, pages 3319–3328. PMLR, 2017.

[39] Avanti Shrikumar, Peyton Greenside, and Anshul Kundaje. Learning important features through propagating activation differences. In *International Conference on Machine Learning*, pages 3145–3153. PMLR, 2017.

[40] Jianlong Zhou, Syed Z Arshad, Kun Yu, and Fang Chen. Correlation for user confidence in predictive decision making. In *Proceedings of the 28th Australian Conference on Computer-Human Interaction*, pages 252–256, 2016.

[41] Ramprasaath R Selvaraju, Michael Cogswell, Abhishek Das, Ramakrishna Vedantam, Devi Parikh, and Dhruv Batra. Grad-cam: Visual explanations from deep networks via gradient-based localization. In *Proceedings of the IEEE international conference on computer vision*, pages 618–626, 2017.

[42] Bolei Zhou, Aditya Khosla, Agata Lapedriza, Aude Oliva, and Antonio Torralba. Learning deep features for discriminative localization. In *Proceedings of the IEEE conference on computer vision and pattern recognition*, pages 2921–2929, 2016.

[43] Aniek F Markus, Jan A Kors, and Peter R Rijnbeek. The role of explainability in creating trustworthy artificial intelligence for health care: a comprehensive survey of the terminology, design choices, and evaluation strategies. *Journal of Biomedical Informatics*, :103655, 2021.

[44] Wojciech Samek, Grégoire Montavon, Andrea Vedaldi, Lars Kai Hansen, and Klaus-Robert Müller. *Explainable AI: interpreting, explaining and visualizing deep learning*, volume 11700. Springer Nature, 2019.

[45] Jianlong Zhou, Amir H Gandomi, Fang Chen, and Andreas Holzinger. Evaluating the quality of machine learning explanations: A survey on methods and metrics. *Electronics*, 10(5):593, 2021.

[46] Jianlong Zhou, Zhidong Li, Huaiwen Hu, Kun Yu, Fang Chen, Zelin Li, and Yang Wang. Effects of influence on user trust in predictive decision making. In *Extended Abstracts of the 2019 CHI Conference on Human Factors in Computing Systems*, pages 1–6, 2019.

[47] Philipp Schmidt and Felix Biessmann. Quantifying interpretability and trust in machine learning systems. *arXiv preprint arXiv:1901.08558*, , 2019.

[48] Sara Hooker, Dumitru Erhan, Pieter-Jan Kindermans, and Been Kim. A benchmark for interpretability methods in deep neural networks. *arXiv preprint arXiv:1806.10758*, , 2018.

[49] An-phi Nguyen and María Rodríguez Martínez. On quantitative aspects of model interpretability. *arXiv preprint arXiv:2007.07584*, , 2020.

[50] Thomas Widmann, Florian Merkle, Martin Nocker, and Pascal Schöttle. Pruning for power: Optimizing energy efficiency in iot with neural network pruning. In *International Conference on Engineering Applications of Neural Networks*, pages 251–263. Springer, 2023.

[51] Hongrong Cheng, Miao Zhang, and Javen Qinfeng Shi. A survey on deep neural network pruning: Taxonomy, comparison, analysis, and recommendations. *IEEE Transactions on Pattern Analysis and Machine Intelligence*, 2024.

[52] Zhuang Liu, Mingjie Sun, Tinghui Zhou, Gao Huang, and Trevor Darrell. Rethinking the value of network pruning. *arXiv preprint arXiv:1810.05270*, , 2018.

[53] Xinrui Jiang, Nannan Wang, Jingwei Xin, Xiaobo Xia, Xi Yang, and Xinbo Gao. Learning lightweight super-resolution networks with weight pruning. *Neural Networks*, 144:21–32, 2021. ISSN 0893-6080. doi:<https://doi.org/10.1016/j.neunet.2021.08.002>. URL <https://www.sciencedirect.com/science/article/pii/S0893608021003075>.

[54] Yann LeCun, John Denker, and Sara Solla. Optimal brain damage. *Advances in Neural Information Processing Systems (NIPS)*, 2, 1989.

[55] Davis Blalock, Jose Javier Gonzalez Ortiz, Jonathan Frankle, and John Guttag. What is the state of neural network pruning? *arXiv preprint arXiv:2003.03033*, , 2020.

[56] Jonathan Frankle and Michael Carbin. The lottery ticket hypothesis: Finding sparse, trainable neural networks. *arXiv preprint arXiv:1803.03635*, , 2018.

[57] Song Han, Jeff Pool, John Tran, and William J Dally. Learning both weights and connections for efficient neural networks. *arXiv preprint arXiv:1506.02626*, , 2015.

[58] Florian Merkle, Maximilian Samsinger, and Pascal Schöttle. Pruning in the face of adversaries. In *The 21st International Conference on Image Analysis and Processing (ICIAP)*, 2022.

[59] Nima Aghli and Eraldo Ribeiro. Combining weight pruning and knowledge distillation for cnn compression. In *2021 IEEE/CVF Conference on Computer Vision and Pattern Recognition Workshops (CVPRW)*, pages 3185–3192, 2021. doi:10.1109/CVPRW53098.2021.00356.

[60] Yang He, Guoliang Kang, Xuanyi Dong, Yanwei Fu, and Yi Yang. Soft filter pruning for accelerating deep convolutional neural networks. *arXiv preprint arXiv:1808.06866*, , 2018.

[61] Zehao Huang and Naiyan Wang. Data-driven sparse structure selection for deep neural networks. In *Proceedings of the European conference on computer vision (ECCV)*, pages 304–320, 2018.

[62] Tianyun Zhang, Shaokai Ye, Kaiqi Zhang, Jian Tang, Wujie Wen, Makan Fardad, and Yanzhi Wang. A systematic dnn weight pruning framework using alternating direction method of multipliers. In *Proceedings of the European Conference on Computer Vision (ECCV)*, pages 184–199, 2018.

[63] Trevor Gale, Erich Elsen, and Sara Hooker. The state of sparsity in deep neural networks. *arXiv preprint arXiv:1902.09574*, , 2019.

[64] Wojciech Samek, Alexander Binder, Grégoire Montavon, Sebastian Lapuschkin, and Klaus-Robert Müller. Evaluating the visualization of what a deep neural network has learned. *IEEE transactions on neural networks and learning systems*, 28(11):2660–2673, 2016.

[65] Reza Abbasi-Asl and Bin Yu. Interpreting convolutional neural networks through compression. *arXiv preprint arXiv:1711.02329*, , 2017.

[66] Marissa Dotter and Chris M Ward. Visualizing compression of deep learning models for classification. In *2018 IEEE Applied Imagery Pattern Recognition Workshop (AIPR)*, pages 1–8. IEEE, 2018.

[67] Yuxin Zhang, Mingbao Lin, Chia-Wen Lin, Jie Chen, Feiyue Huang, Yongjian Wu, Yonghong Tian, and Rongrong Ji. Channel pruning in a white box for efficient image classification, 2021.

[68] Seul-Ki Yeom, Philipp Seegerer, Sebastian Lapuschkin, Alexander Binder, Simon Wiedemann, Klaus-Robert Müller, and Wojciech Samek. Pruning by explaining: A novel criterion for deep neural network pruning. *Pattern Recognition*, 115:107899, 2021.

[69] Kimia Soroush, Mohsen Raji, and Behnam Ghavami. Compressing deep neural networks using explainable ai. In *2023 13th International Conference on Computer and Knowledge Engineering (ICCKE)*, pages 636–641. IEEE, 2023.

[70] Sebastian Bach, Alexander Binder, Grégoire Montavon, Frederick Klauschen, Klaus-Robert Müller, and Wojciech Samek. On pixel-wise explanations for non-linear classifier decisions by layer-wise relevance propagation. *PLoS one*, 10(7):e0130140, 2015.

[71] Muhammad Sabih, Frank Hannig, and Juergen Teich. Utilizing explainable ai for quantization and pruning of deep neural networks. *arXiv preprint arXiv:2008.09072*, , 2020.

[72] Kaixuan Yao, Feilong Cao, Yee Leung, and Jiye Liang. Deep neural network compression through interpretability-based filter pruning. *Pattern Recognition*, :108056, 2021.

[73] Matthew D Zeiler and Rob Fergus. Visualizing and understanding convolutional networks. In *European conference on computer vision*, pages 818–833. Springer, 2014.

[74] Lu Yu and Wei Xiang. X-pruner: explainable pruning for vision transformers. In *Proceedings of the IEEE/CVF conference on computer vision and pattern recognition*, pages 24355–24363, 2023.

[75] Praboda Rajapaksha and Noel Crespi. Explainable attention pruning: A meta-learning-based approach. *IEEE Transactions on Artificial Intelligence*, 2024.

[76] Jonathan Frankle and David Bau. Dissecting pruned neural networks. In *ICLR 2019 Debugging Machine Learning Models Workshop*. MIT CSAIL, 2019. Presented at ICLR 2019 Debugging Machine Learning Models Workshop.

[77] David Bau, Bolei Zhou, Aditya Khosla, Aude Oliva, and Antonio Torralba. Network dissection: Quantifying interpretability of deep visual representations. In *Proceedings of the IEEE conference on computer vision and pattern recognition*, pages 6541–6549, 2017.

[78] Eric Arazo, Hristo Stoev, Cristian Bosch, Andrés L Suárez-Cetrulo, and Ricardo Simón-Carbajo. Xpression: A unifying metric to optimize compression and explainability robustness of ai models. In *World Conference on Explainable Artificial Intelligence*, pages 370–382. Springer, 2024.

[79] Chih-Kuan Yeh, Cheng-Yu Hsieh, Arun Suggala, David I Inouye, and Pradeep K Ravikumar. On the (in) fidelity and sensitivity of explanations. *Advances in neural information processing systems*, 32, 2019.

[80] Jia Deng, Wei Dong, Richard Socher, Li-Jia Li, Kai Li, and Li Fei-Fei. Imagenet: A large-scale hierarchical image database. In *2009 IEEE conference on computer vision and pattern recognition*, pages 248–255. Ieee, 2009.

[81] Jeremy Howard. Imagenette, 2019. URL <https://github.com/fastai/imagenette/>.

[82] Karen Simonyan and Andrew Zisserman. Very deep convolutional networks for large-scale image recognition. *arXiv preprint arXiv:1409.1556*, , 2014.

[83] Michela Paganini and Jessica Forde. Streamlining tensor and network pruning in pytorch. *arXiv preprint arXiv:2004.13770*, , 2020.

[84] Pavlo Molchanov, Stephen Tyree, Tero Karras, Timo Aila, and Jan Kautz. Pruning convolutional neural networks for resource efficient inference. In *5th International Conference on Learning Representations, ICLR 2017, Toulon, France, April 24-26, 2017, Conference Track Proceedings*. OpenReview.net, 2017. URL <https://openreview.net/forum?id=SJGCiw5gl>.

[85] Aravindh Mahendran and Andrea Vedaldi. Visualizing deep convolutional neural networks using natural pre-images. *CoRR*, abs/1512.02017, 2015. URL <http://arxiv.org/abs/1512.02017>.

[86] Yoshua Bengio, Aaron C. Courville, and Pascal Vincent. Unsupervised feature learning and deep learning: A review and new perspectives. *CoRR*, abs/1206.5538, 2012. URL <http://arxiv.org/abs/1206.5538>.

[87] Aditya Chattopadhyay, Anirban Sarkar, Prantik Howlader, and Vineeth N Balasubramanian. Grad-cam++: Generalized gradient-based visual explanations for deep convolutional networks. *2018 IEEE Winter Conference on Applications of Computer Vision (WACV)*, , Mar 2018. doi:10.1109/wacv.2018.00097. URL <http://dx.doi.org/10.1109/WACV.2018.00097>.

[88] Klaus Krippendorff. Computing krippendorff's alpha-reliability, 2011. Retrieved from: https://repository.upenn.edu/asc_papers/43 [accessed: January 10, 2025].

[89] Heimo Müller and Andreas Holzinger. Kandinsky patterns. *Artificial intelligence*, 300:103546, 2021.

[90] Kaiming He, Xiangyu Zhang, Shaoqing Ren, and Jian Sun. Deep residual learning for image recognition. In *Proceedings of the IEEE conference on computer vision and pattern recognition*, pages 770–778, 2016.

[91] Christian Szegedy, Wei Liu, Yangqing Jia, Pierre Sermanet, Scott Reed, Dragomir Anguelov, Dumitru Erhan, Vincent Vanhoucke, and Andrew Rabinovich. Going deeper with convolutions. In *Proceedings of the IEEE conference on computer vision and pattern recognition*, pages 1–9, 2015.

[92] Mingxing Tan and Quoc Le. Efficientnet: Rethinking model scaling for convolutional neural networks. In *International Conference on Machine Learning*, pages 6105–6114. PMLR, 2019.

[93] Ze Liu, Yutong Lin, Yue Cao, Han Hu, Yixuan Wei, Zheng Zhang, Stephen Lin, and Baining Guo. Swin transformer: Hierarchical vision transformer using shifted windows. In *International Conference on Computer Vision (ICCV)*, 2021.

[94] Alexey Dosovitskiy, Lucas Beyer, Alexander Kolesnikov, Dirk Weissenborn, Xiaohua Zhai, Thomas Unterthiner, Mostafa Dehghani, Matthias Minderer, Georg Heigold, Sylvain Gelly, Jakob Uszkoreit, and Neil Houlsby. An image is worth 16x16 words: Transformers for image recognition at scale. *ArXiv*, abs/2010.11929, 2021.

A Additional Material from the Pre-study

Figures 12 and 13 demonstrate the experimental setup of the pre-study.

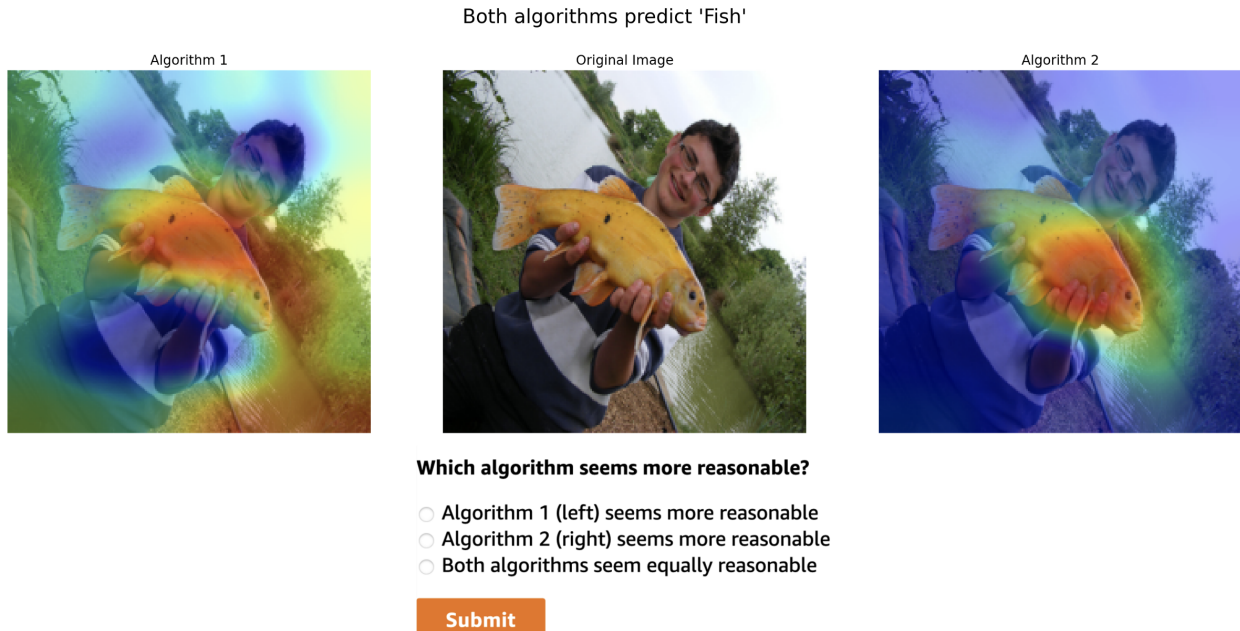


Figure 12: Experimental Pre-study setup with heat maps CR 32 (left) vs. CR 1 (right).

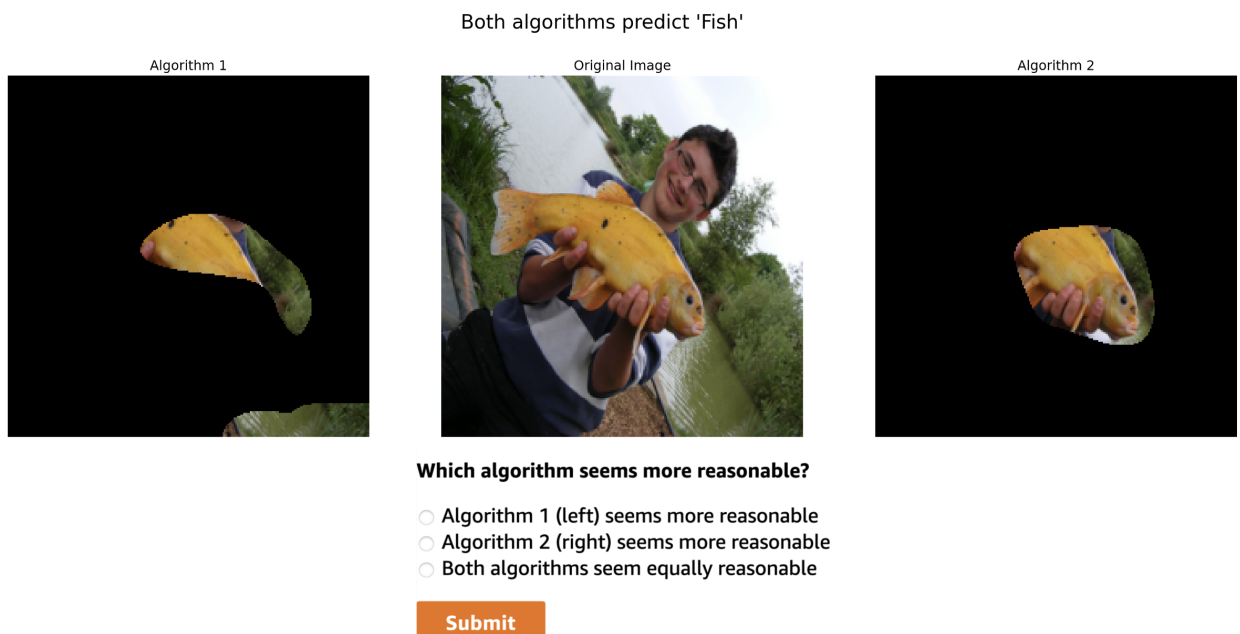


Figure 13: Experimental Pre-study setup with occlusion maps CR 32 (left) vs. CR 1 (right).

B Additional Material from Experiment 1

Figure 14 demonstrates the distribution of the answers for each CR in Experiment 1. The change in distribution is clearly visible between the CRs. Figure 15 provides an aggregated view of these results.

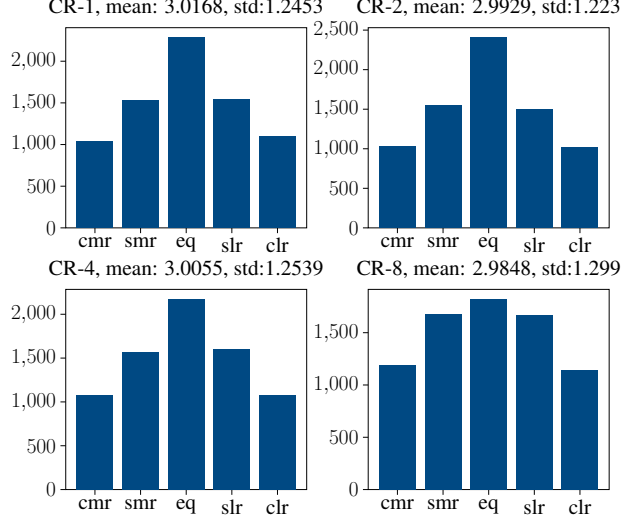


Figure 14: The distribution of each stacked bar from Figure 15.

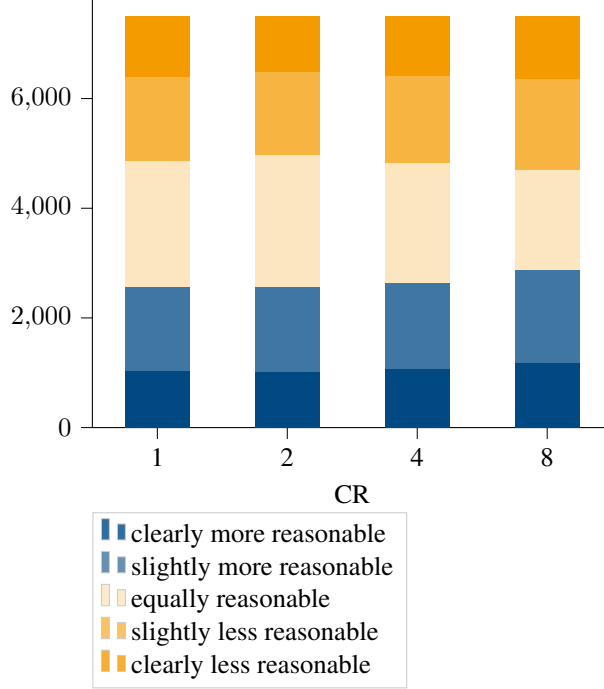


Figure 15: Aggregated results of Experiment 1 for all CRs.

C Additional Material from Experiment 2

Figures 16 (CR 4), 17 (CR 8), and 18 (CR 32) complement the previous confusion matrices presented in section 4.3. Darker values indicate lower numbers, lighter values indicate higher numbers. The diagonals display correct classifications, while the right-most column shows the number of 'I don't know / None of the above'.

Together with CR 8, CR 4 has the highest error-rate (5.36%). The highest indecisiveness and error-rate is given for class 'chain saw' across all CR. CR 8 demonstrated the lowest accuracy in Experiment 2 (81.2%). CR 32 achieved the highest indecisiveness (14.2%) and second lowest accuracy in Experiment 2 (81.32%). To summarize, table 8 provides an overview of indecisiveness per class and CR.

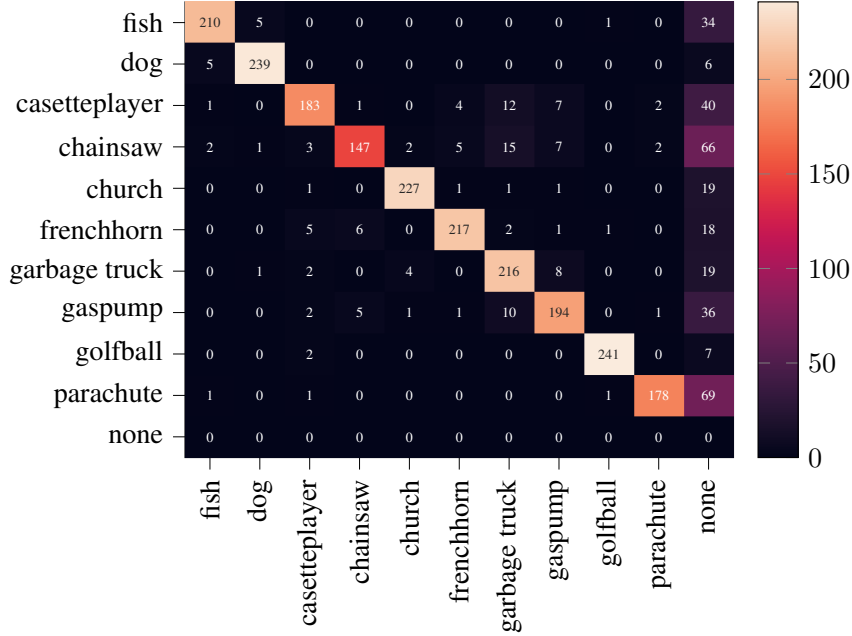


Figure 16: Confusion Matrix CR 4.

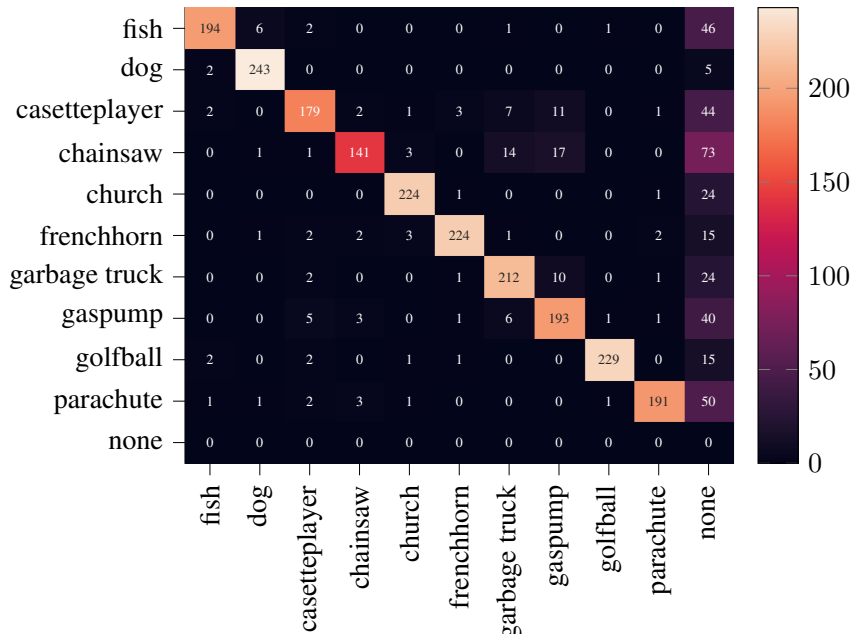


Figure 17: Confusion Matrix CR 8.

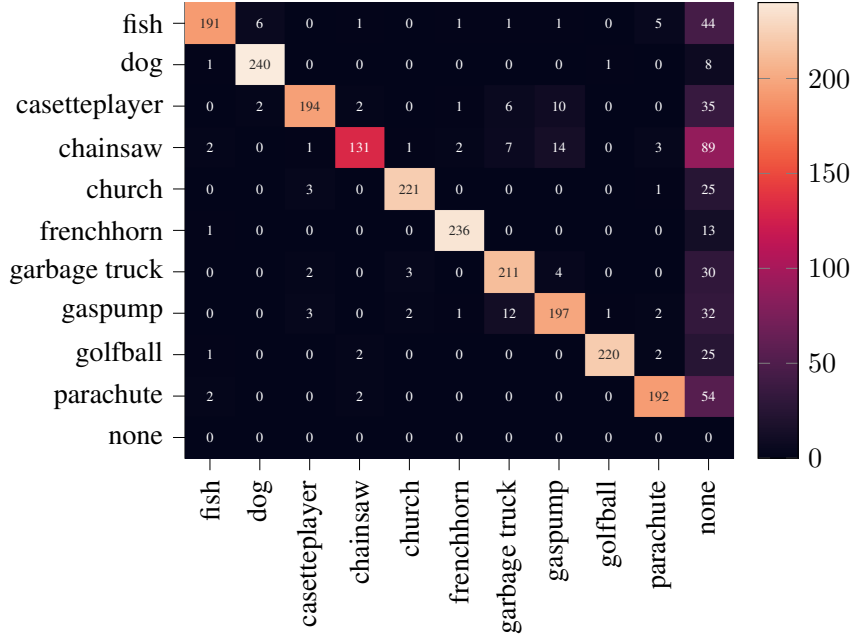


Figure 18: Confusion Matrix CR 32.

	CR 1	CR 2	CR 4	CR 8	CR 32
fish	6.8%	7.2%	13.6%	18.4%	17.6%
dog	8.8%	4.0%	2.4%	2.0%	3.2%
cassette player	13.2%	12.0%	16.0%	17.6%	14.0%
chainsaw	22.4%	22.0%	26.4%	29.2%	35.6%
church	12.8%	3.6%	7.6%	9.6%	10.0%
french horn	4.0%	3.2%	7.2%	6.0%	5.2%
garbage truck	7.2%	5.2%	7.6%	9.6%	12.0%
gas pump	11.6%	14.8%	14.4%	16.0%	12.8%
golfball	2.4%	1.6%	2.8%	6.0%	10.0%
parachute	8.8%	16.0%	27.6%	20.0%	21.6%
total	9.80%	8.96%	12.56%	13.44%	14.20%

Table 8: Indecisiveness of the respondents per class for all CRs.